Monthly Notices
of the
ROYAL ASTRONOMICAL SOCIETY

MNRAS **488,** 2158–2174 (2019)
Advance Access publication 2019 June 25

doi:10.1093/mnras/stz1710

Young star clusters and the structure of the second Galactic quadrant II

J. A. Molina Lera,★ G. Baume ★ and R. Gamen★

Instituto de Astrofísica de La Plata (CONICET–UNLP), and Facultad de Ciencias Astronómicas y Geofísicas (UNLP), Paseo del Bosque s/n, La Plata B1900FWA, Argentina

Accepted 2019 June 18. Received 2019 June 18; in original form 2019 April 1

ABSTRACT

Galactic spiral arms are traced using young objects as giant molecular clouds, H II regions, OB stars, or young open/embedded clusters. To improve the knowledge of the Galactic structure in the second quadrant we selected, from more than 200 open clusters covered by the SDSS, a sample of 10 young stellar clusters to conduct a spectrophotometric study.

Photometric data were provided by SDSS and APASS in the optic bands and by 2MASS and WISE in the infrared. Spectroscopic information was obtained from observations acquired with GMOS/GEMINI complemented with data from the literature. For six of the 10 clusters, distances were also obtained with our astrometric *Gaia* data analysis. To perform all tasks we used a suite of tools developed by us.

Our results show that these open clusters are distributed along three spiral arms, covering distances from 1.8 to 8.0 kpc. We confirm, using our novel spectroscopic data, our previews photometric estimations regarding the Galactic location of the cluster Teutsch 45. We found that it is located beyond the 'Outer Arm' and probably belong to the more distant 'New Arm' extending its trace almost to the anticentre. Hence, it was possible to get a better picture of the structure of the outer regions of the Galaxy. For clusters with pre-main-sequence populations we also found traces of coeval star formation processes. Regarding spectroscopic data and most massive members of the clusters, we discovered seven B-type stars, all earlier than B4 and we also confirmed the spectral classification of one O8-8.5 type star.

Key words: stars: early-type – stars: formation – open clusters and associations: general – Galaxy: structure.

1 INTRODUCTION

Main design of Galactic spiral arms is well traced using young objects as giant molecular clouds, H II regions, OB stars, or young open/embedded clusters. The estimation of their distances provides a big picture of the Galactic structure and several works have been developed with this objective (Carraro 2014). These structures should be explained by numerical simulations and analytic theories (Grosbøl & Carraro 2018). Additionally, several models have been proposed to describe the path followed by the main spiral arms (see for example Hou & Han 2014; Vallée 2017). Despite the efforts made, controversy still remains about important features as the number of main arms. While some works claim for a model with two main arms (see Benjamin et al. 2005), others for a model with four ones (see Camargo, Bonatto & Bica 2015). There could also be undiscovered minor inter-arm features similar to those seen on external galaxies (Elmegreen 1980). Examples in the Milky Way are the 'Orion spur', the Giant molecular filaments identified by Abreu-Vicente et al. (2016) in the fourth Galactic quadrant, and the particular description of Carina region given by Carraro et al. (2017). It is also unclear how far the star formation regions extend to the outer regions of the Galaxy. In particular, it is interesting to trace the external region of the second Galactic quadrant (2GQ) where there are several evidences of the presence of an identified 'New Arm' located behind the already know 'Outer Arm' (see Sun et al. 2015; Molina Lera et al. 2018, for details and references therein).

Based on the aforementioned ideas considering the importance of tracing the structure in the outer zones of the Milky Way, we started an analysis of known young open clusters of the 2GQ with available photometric optical data from the Sloan Digital Sky Survey (SDSS; Ahn et al. 2012[1]), whose first results were presented in Molina Lera et al. (2018). In this case we selected and analysed a new sample of 10 open clusters located in the 2GQ (see Fig. 1)

★ E-mail: jalejoml@fcaglp.unlp.edu.ar (JAML); gbaume@fcaglp.unlp.edu.ar (GB); rgamen@fcaglp.unlp.edu.ar (RG)

[1]This survey covers several stripes 2.5-deg wide in the Galactic plane at the 2GQ.

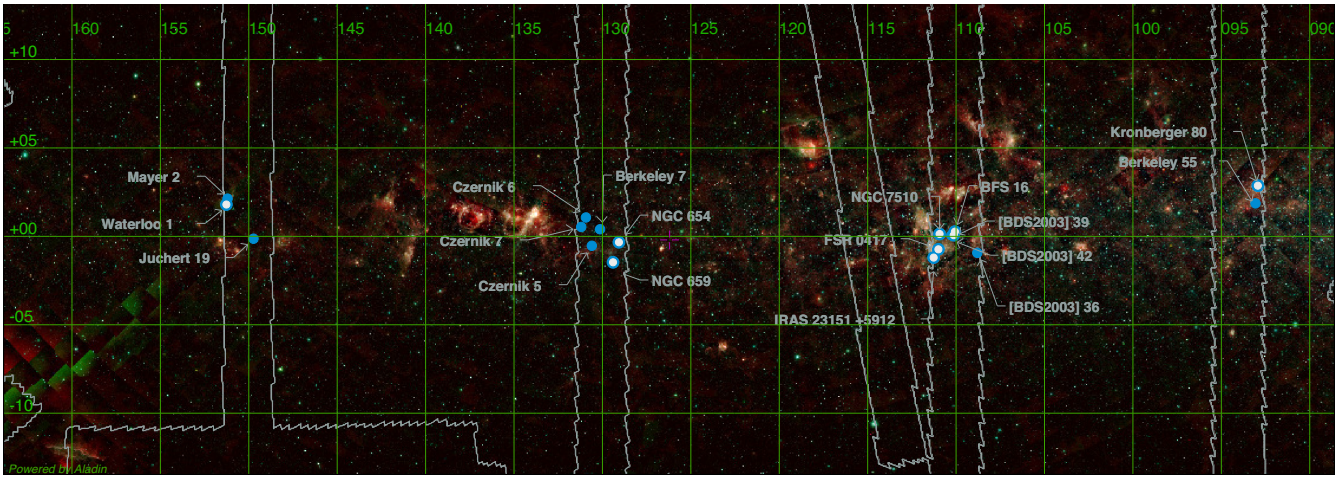

Figure 1. All-sky WISE image covering the whole 2GQ around the Galactic plane. The white lines indicate strip regions covered by the SDSS. The blue and white filled circles are the star clusters studied in this work. The blue filled circles are the star clusters presented in Molina Lera, Baume & Gamen (2018).

Table 1. Photometric zero-point (*zp*) and *rms* values for each studied cluster region.

Cluster	Band	*zp*	*rms*
Teutsch 45	*u*	9.03 ± 0.01	0.03
	g	9.11 ± 0.01	0.02
	r	9.13 ± 0.01	0.04
	i	9.09 ± 0.01	0.02
Waterloo 1	*u*	7.63 ± 0.01	0.09
	g	7.60 ± 0.01	0.08
	r	7.55 ± 0.01	0.02
	i	7.53 ± 0.01	0.05
NGC 659	*u*	8.97 ± 0.01	0.09
	g	8.94 ± 0.01	0.08
	r	9.02 ± 0.01	0.07
	i	9.08 ± 0.01	0.08
NGC 654	*u*	8.88 ± 0.01	0.09
	g	8.70 ± 0.01	0.08
	r	8.89 ± 0.01	0.07
	i	8.88 ± 0.01	0.07
IRAS 23151+5912	*u*	8.27 ± 0.01	0.06
	g	8.36 ± 0.01	0.02
	r	8.34 ± 0.01	0.02
	i	8.27 ± 0.01	0.03
FSR 0417	*u*	8.71 ± 0.01	0.07
	g	8.75 ± 0.01	0.03
	r	8.68 ± 0.01	0.07
	i	8.79 ± 0.01	0.07
NGC 7510	*u*	8.75 ± 0.01	0.06
	g	8.75 ± 0.01	0.03
	r	8.71 ± 0.01	0.04
	i	8.60 ± 0.01	0.06
BFS 16	*u*	9.07 ± 0.01	0.04
	g	9.03 ± 0.01	0.04
	r	9.12 ± 0.01	0.04
	i	8.99 ± 0.01	0.03
[BDS2003] 39	*u*	8.85 ± 0.01	0.04
	g	8.95 ± 0.01	0.04
	r	8.92 ± 0.01	0.04
	i	8.85 ± 0.01	0.04
Kronberger 80	*u*	8.78 ± 0.01	0.05
	g	8.80 ± 0.01	0.04
	r	8.81 ± 0.01	0.06
	i	8.83 ± 0.01	0.04

with the general objective of better tracing the outer spiral structure of the Galaxy.

The paper is organized with the following sections: in Section 2, we present the used data, describing the employed reduction procedures, when it correspond. In Section 3, we summarized our methodology to select the studied clusters and to carry out the estimation of their parameters. In Section 4, we detailed the characteristic of each studied cluster. Finally, in Sections 5 and 6, we present a general discussion of our previous analysis, comparing them with previous results.

2 DATA

2.1 Photometric and astrometic data

We used photometry at *ugri* bands provided by the SDSS-III[2] data release. This catalogue was compiled from observations made in a dedicated 2.5 m f/5 telescope at Apache Point Observatory. However, this catalogue lacks photometric information of the objects located around very bright stars, crowded regions, and several star clusters beside if they are crowded or not. This situation includes several of our targets, therefore we downloaded the corresponding FITS images from SDSS DR12 Science Archive Server (SAS) that were already bias, dark, and flat corrected by the corresponding pipelines (Stoughton et al. 2002). Then, we performed point spread function (PSF) photometry (Stetson 1987) over the images using IRAF/DAOPHOT[3] package to obtain instrumental magnitudes. In the first stage of this procedure we used a 4 pixels (1.″6) aperture in radius and a correction magnitude was computed over each image to carry our measures to a 17 pixels aperture (6.″7). All resulting tables were combined using DAOMASTER code (Stetson 1992). Then, we carried out flux calibration by fitting with the common sources provided by the SDSS catalogues (Alam et al. 2015) and using the IRAF/PHOTPARS package. The obtained zero-point corrections and root mean square (*rms*) values of the fits are indicated in Table 1. Saturated stars were complemented, when available, with *gri* data

[2] http://www.sdss3.org/

[3] IRAF is distributed by the National Optical Astronomy Observatories, which are operated by the Association of Universities for Research in Astronomy, Inc., under cooperative agreement with the National Science Foundation.

Table 2. Fundamental parameters of the studied star clusters.

Name	Centre		Radius	$\rho_\circ/\rho_{out}$	$E_{(B-V)}$	δ	$V_\circ - M_V$	Age (Myr)	
	$\alpha_{J2000.0}$	$\delta_{J2000.0}$	(′)		(mag)	(mag)		Nuclear	Contraction
Teutsch 45	05:42:46.4	30:57:39.9	2.6	3.0	0.95	0.20	14.5	1–3	1–3
Waterloo 1	04:18:43.4	52:52:08.8	2.6	2.0	0.85	0.25	12.9	3–10	–
NGC 659	01:44:23.5	60:40:25.7	3.5	4.6	0.80	0.25	12.5	10–30	∼ 10
NGC 654	01:43:59.7	61:53:08.0	10.2	3.4	0.75	0.30	12.5	∼30	10–30
IRAS 23151+5912	23:17:17.3	59:28:35.2	1.9	1.7	0.80	0.30	12.5	∼ 30	∼ 30
FSR 0417	23:13:58.3	59:49:28.1	6.4	4.8	0.85	0.25	12.5	3–10	10–30
NGC 7510	23:11:04.6	60:34:29.8	4.1	5.9	1.00	0.30	12.5	10–30	∼ 10
[BDS2003] 39	23:05:10.1	60:14:31.0	1.5	6.0	1.75	0.50	11.3	1–3	–
BFS 16	23:03:25.1	60:22:36.3	2.4	5.0	1.10	0.30	11.8	3–10	–
Kronberger 80	21:11:49.4	52:22:43.7	2.3	5.0	2.60	0.50	14.2	10–30	–

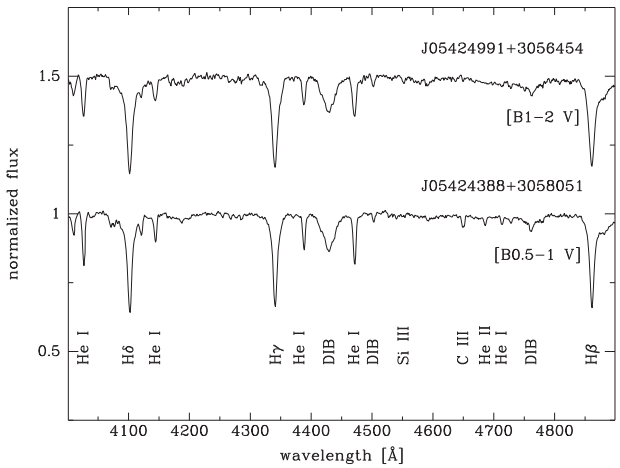

Figure 2. Optical spectra obtained for the two B-type stars in Teutsch 45. Object identifications, spectral classifications, and most noticeable features are labelled.

from the APASS Data Release 9 (Henden et al. 2015) catalogue for most cases, and for a few stars we used SIMBAD data base. Finally, we correlated the optical photometric data with several catalogues obtained from sky surveys as the Two Micron All-Sky Survey (2MASS; Strutskiw et al. 2006), the Wide-field Infrared Survey Explorer (WISE; Wright et al. 2010), and the *Gaia* Data Release 2 (DR2; Gaia Collaboration 2016; Brown et al. 2018). The two former catalogues provided photometric data at J, H, K and 3.4, 4.6, 12, and 22 μm ($W1$, $W2$, $W3$, $W4$) infrared bands, whereas the latter contains astrometric information together with photometric data at particular bands G, G_{BP}, and G_{RP}.

2.2 Spectroscopic data

Spectroscopic information of the stars in the clusters were searched in the SIMBAD[4] data base. Since several clusters lacked of such information we obtained new spectroscopic data using poor weather time at Gemini North. Based on our preliminary photometric analysis (see Section 2.1), we selected some objects with high probability to be early-type stars, and observe them with the Gemini Multi-Object Spectrograph (GMOS[5]) during nights of 2018 December (proposal ID: GN-2018B-Q-408; PI: JAML).

[4]http://simbad.u-strasbg.fr/simbad/
[5]http://www.gemini.edu/sciops/instruments/gmos/

GMOS was set in its long-slit mode and a 1-arcsec-width slit covering at least two stars at each observation. To avoid the inter CCDs gaps in the spectral images, we employed the B600 grid centred at 5200 and 5250 Å. We finally obtained spectra with a wavelength coverage from 3700 to 6800 Å, a resolving power $R \sim 1000$ and typical signal-to-noise ratios $SNR \sim 120$ (although some spectra reached just up to 80).

We performed the reduction procedure using IRAF packages and the instructions given by the Gemini Observatory. Next, the new own spectra were qualitatively classified comparing them with the standard ones given by Walborn & Fitzpatrick (1990) and Sota et al. (2011, 2014).

3 METHODOLOGY

With the idea to perform a uniform and homogeneous study, we used the criteria of object selection and subsequent analysis following the main guidelines described at our previous work (Molina Lera et al. 2018) to which we add, for this new sample of open clusters, results obtained from an analysis conducted with *Gaia* DR2. In brief, the object selection was based on mainly poorly studied clusters at the 2GQ catalogued by the 'Milky Way global survey of star clusters' (MWSC; Kharchenko et al. 2013) and/or by the 'New infrared star clusters in the Northern and Equatorial Milky Way with 2MASS' (Bica et al. 2003) with relevant stellar overdensities and also covered by the SDSS. Regarding the analysis of each cluster region, we simultaneously drew the attention on the spatial location of the stars, their place over all the photometric diagrams and took into account their corresponding spectral classification (see details in Molina-Lera et al. 2016 and Molina Lera et al. 2018). That is, we first selected probable cluster members based on the stellar density maps constructed with sources in the J band ($J < 15$) in most cases (particular cases are mentioned in each cluster, see Section 4). For each region we computed the ratios ($\rho_\circ/\rho_{out}$) between the peak density value and a representative one of the field density. Then, the photometric and spectroscopic information allowed us to characterize three different stellar populations on each studied cluster with the following rules:

(i) Upper main sequence (UMS): Sources located between two envelope curves placed around the best-fitting ZAMS on the ($u - g$) versus ($g - r$) and the g versus ($u - g$) diagrams. Shifting (δ) values were adopted taking into account the differential reddening and/or possible evolution effects (see Table 2).

(ii) Pre-main-sequence populations (PMS): Objects located to the right of the reddening curve drawn on the IR TCDs.

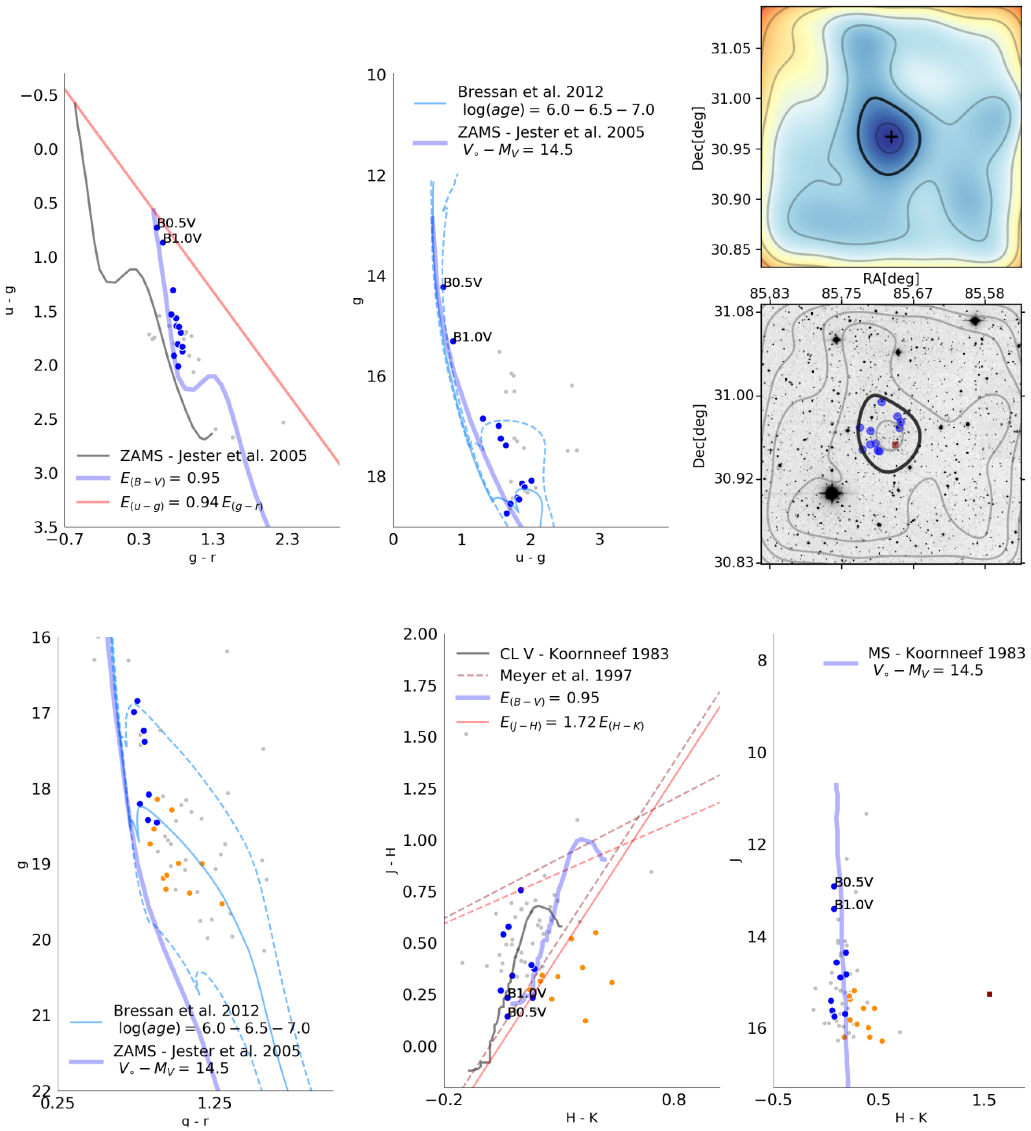

Figure 3. Teutsch 45. Top right: Stellar density map where bluest colours indicate the highest density values. 2MASS *J* band image with grey curves correspond to iso-density stellar values and black curve with the selected mean stellar value. The cross indicates the regions centre and blue circles are selected UMS stars. Photometric diagrams; black and blue curves correspond to MS or ZAMS reference stars. The continuous red lines represent the reddening direction. The red dotted lines show Meyer et al. (1997) criterion. Bressan et al. (2012) isochronous are shown as light blue curves. The blue circles indicate selected UMS stars and orange circles are selected PMS candidates (see the text for details). The dark blue squares are stars used in *Gaia* data analysis.

(iii) Abnormally reddened sources or those which correspond to the classical T-Tauri stars (dark red squares): Sources that follow the criteria given by Meyer, Calvet & Hillenbrand (1997).

In particular, for stars with spectral classification, we could apply the colour difference method to estimate the selective absorption coefficient ($R_V = A_V/E_{B-V}$). The obtained results were compared with those ratios corresponding to the relative absorption values r_X given by Cardelli, Clayton & Mathis (1989) for a B5 V type star. We noticed high different values inside some clusters and others have only one star with spectral classification, therefore we adopted a normal reddening ($R_V = 3.1$) for all the clusters. Notwithstanding, to estimate the influence of this assumption over our results in distances and reddening, we also conducted a study of the distribution of UMS in the photometric diagrams for R_V values equal to 2.9 and 3.4. The obtained results are mentioned in Section 5.

Spectrophometric distances and colour excess were calculated using the traditional spectrophotometric technique from certain spectral type (ST) stars. These stars are marked with an asterisk in Table 3. Nevertheless all compiled stars for this work with spectral information are listed in the mentioned table. Absolute visual magnitude (M_V) and intrinsic colour calibrations were adopted from Sung et al. (2013). We used these values as reference to estimate the fundamental parameters from the analysis of the star distribution over the photometric diagrams.

We also used astrometric information provided by *Gaia* DR2 to estimate cluster distances. To perform this task we took into account the considerations given by Cantat-Gaudin et al. (2018) and the guidelines regarding proper motion analysis indicated by

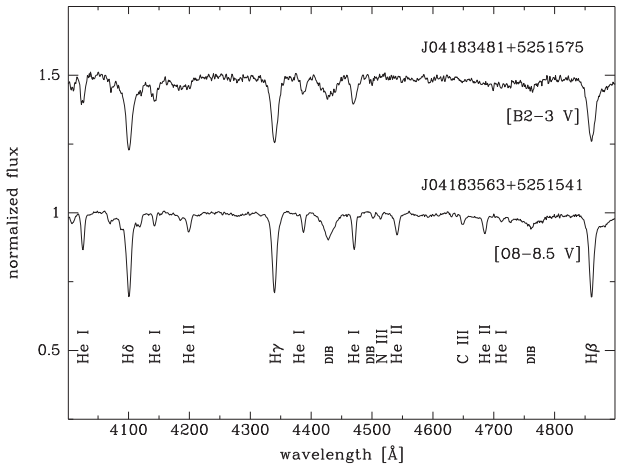

Figure 4. Optical spectra obtained for the OB stars in Waterloo 1. Object identifications, spectral classifications, and most noticeable features are labelled.

Baume et al. (2011). In brief, we added +0.029 mas to all parallax values and then computed for each cluster region an error weighted average ($Plx_{\rm avg}$) of the individual parallaxes values of selected stars. This selection of stars was done considering those ones with the lowest relative errors in parallaxes and proper motions ($e_{\rm plx}/plx < 0.2$ and $e_{\rm pm}/pm < 0.15$), and also located in the corresponding cluster overdensity (defined from an adopted threshold value) in the vector point diagram (μ_δ vs. $-\mu_\alpha\, cos(\delta)$). The errors in $Plx_{\rm avg}$ values were computed as the standard deviations ($std_{\rm plx}$) of the individual parallaxes in the selected sample for each cluster, while the corresponding distances were obtained as $d = 1/Plx_{\rm avg}$ with the upper and lower limits given as $1/(Plx_{\rm avg} \mp std_{\rm plx})$. These calculated errors must be considered, taking into account the remarks given by Bailer-Jones (2015).

We were able to derive reliable distances using *Gaia* data for six of the 10 open clusters presented in this paper. In the other cases we did not find concluding results due to the small amount of stars and/or the lack of *Gaia* data for specific ones. We used the obtained distances as a strong references when pondering the results from the spectrophotometric calculation and the estimated values from the distribution of the UMS in the photometric diagrams. The latter are the ones listed in the Table 2. Selected *Gaia* stars are shown with dark blue squares in all six clusters photometric diagrams. Only a few of these stars are situated far from their expected location on the photometric diagrams. This effect could be caused by saturated values on the SDSS images. In Section 4, an individual description of each cluster is made, presenting the results obtained from the spectroscopic and *Gaia* data analysis, and finally the photometric estimates. We also used isochrones for pre- and post-main-sequence stellar populations from Bressan et al. (2012) to estimate the nuclear and, when it was possible, contraction ages by comparison with the data on the CMDs.

All the tasks indicated before were carried out using a special code developed in PYTHON language (see Molina Lera et al. 2018 for more details). It includes data acquisition, catalogues correlation, centre and size estimations, photometric/spectroscopic analysis, selection of particular stellar populations, and finally, estimation of main cluster parameters.

4 SELECTED STAR CLUSTERS

4.1 Teutsch 45

Previous studies about Teutsch 45, as the MWSC and Bonatto & Bica (2010), have discrepancies regarding its fundamental parameters: an age of 10 Myr, a distance ranging from 3 to 7 kpc ($V_\circ - M_V =$ 12.4–14.2) and colour excess (E_{B-V}) values from 0.75 to about 1.0. Molina Lera et al. (2018) analysed this cluster, using optical (*ugri*) and IR (*JHK*) photometric data, and estimated values for excess colour ($E_{(B-V)} = 0.95$), distance module ($V_\circ - M_V = 14.5$), and a nuclear age (1–3 Myr). In this work we complemented our previous photometric data with spectroscopic observations which revealed two massive stars in the cluster identified as 2MASS J05424388+3058051 and 2MASS J05424991+3056454 that were classified as B0.5-1 V and B1-2 V, respectively.

In particular, 2MASS J05424388+3058051 star presents C III λλ4647/50/51 and He II λ4686 lines, indicating an early-B. The noisier spectrum of J05424991+3056454 star does not present those lines, then a later type was considered. On the other hand, no Mg II λ4481 line was detected but Si III λ4552 line was marginally noticed, then it should be earlier than B2.5.

The spectra of these new B-type stars are shown in Fig. 2. Thus, we were able to calculate the mean spectrophotometric colour excess and distance module, yielding, respectively, the $E_{(B-V)} = 1.0$ and $V_\circ - M_V = 14.6$ (8.3 kpc) values.

In Fig. 3 we present the corresponding stellar density map, from which we obtained an overdensity ratio $\rho_\circ/\rho_{\rm out} \approx 3$. Photometric diagrams were constructed with the same cluster parameters (distance, colour excess, and ages) as those presented in the cited paper. It could be seen that previews photometric results predicted the ones calculated using the spectrophotometric technique. From the isochrone fitting we also estimated a nuclear age of 1–3 Myr. Diagrams also suggest the presence of a PMS population (orange circles) that corresponds to a contraction age of 1–3 Myr.

4.2 Waterloo 1

Waterloo 1 cluster was first studied by Moffat, Jackson & Fitzgerald (1979) using *UBV* photometry and MK spectroscopy. They catalogued BD +52 805 (= ALS 7928) star as an O9.5 star and calculated a distance value of 4.4 kpc ($V_\circ - M_V = 13.2$) and a colour excess of $E_{(B-V)} = 0.9$. The MWSC presents the same values regarding distance and reddening and also an age of ∼ 400 Myr. Recently, Cantat-Gaudin et al. (2018), using *Gaia* DR2, established a 'most likely distance' (dmode) of 4.1 kpc.

We conducted spectroscopic observations over two of the brightest stars in the cluster (Fig. 4). One of them is identified as 2MASS J04183563+5251541 (= BD + 52 805) and we classified it as an O8-8.5 V in agreement with the Galactic O-Star Catalogue (GOSC; Maíz Apellániz et al. 2016) where it is classified as O8 V(n). The other star identified as 2MASS J04183481+5251575 was classified as a B2-3 V since He I lines are well identified but there are no He II or Si III or Mg II. Additionally, the 2MASS J04183950+5250550 star is classified as a B1.5V star in SIMBAD. Therefore, we could compute the spectrophotometric distance module and colour excess for these three UMS stars, considering a O8 V for the O8-8.5 V star and a B2 V for the B2-3 V. The averaged values for distance modulus was 12.95 (3.8 kpc) and a colour excess in $B - V$ of 0.9.

Since it is a small and tenuous cluster, stellar density maps for this region were constructed using sources as faint as $J = 17$.

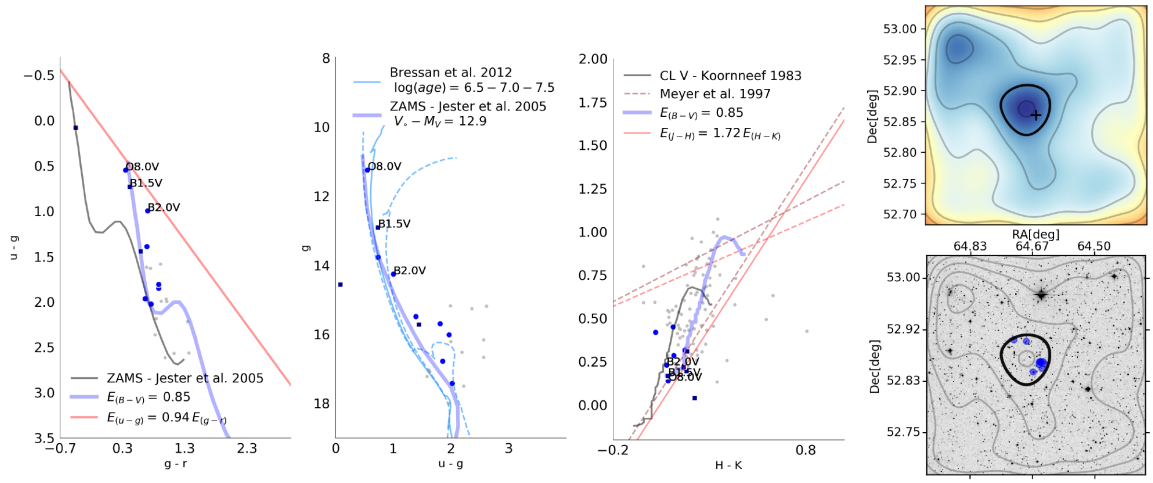

Figure 5. Waterloo 1. Similar description to Fig. 3. The dark blue squares are stars used in *Gaia* data analysis.

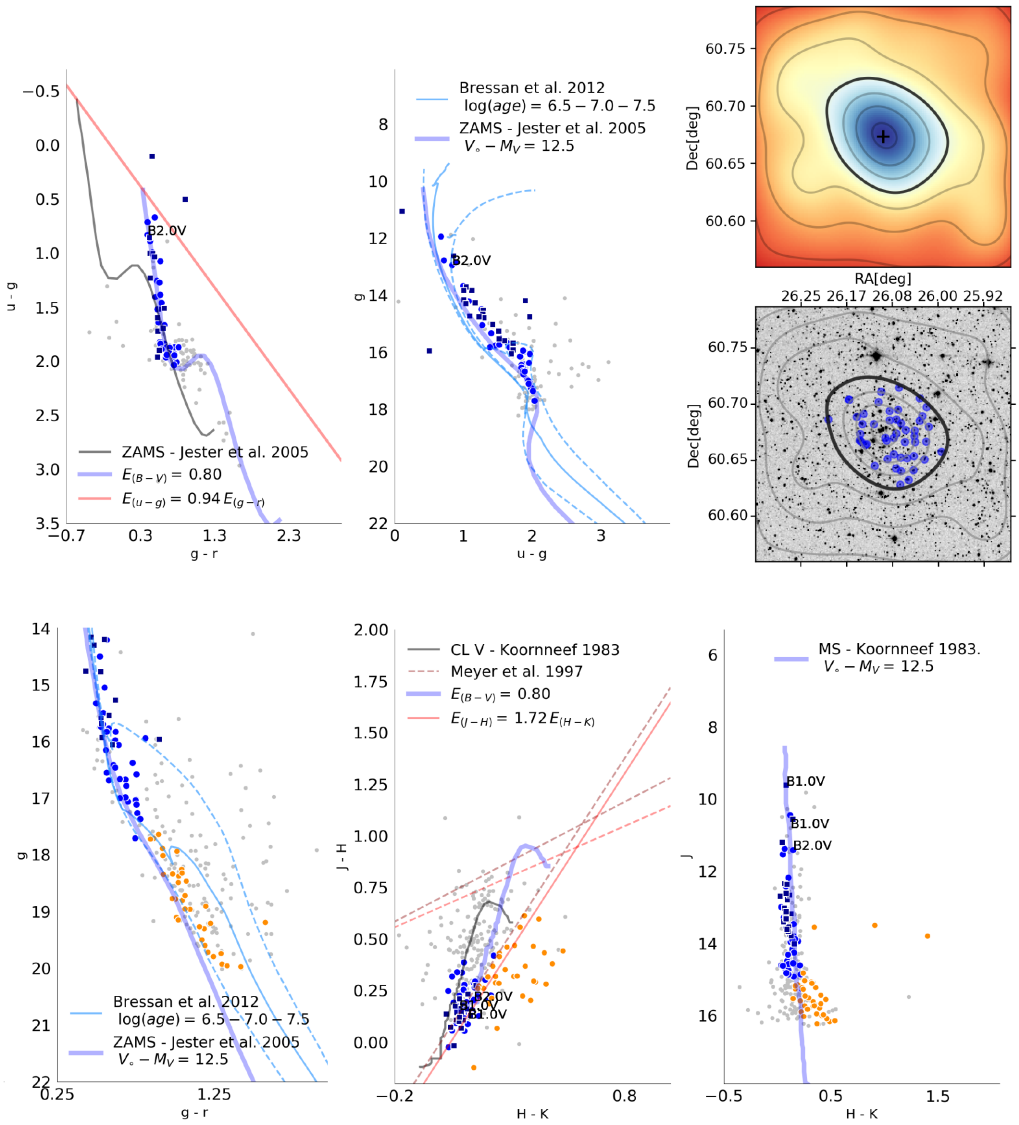

Figure 6. NGC 659. Similar description to Fig. 3.

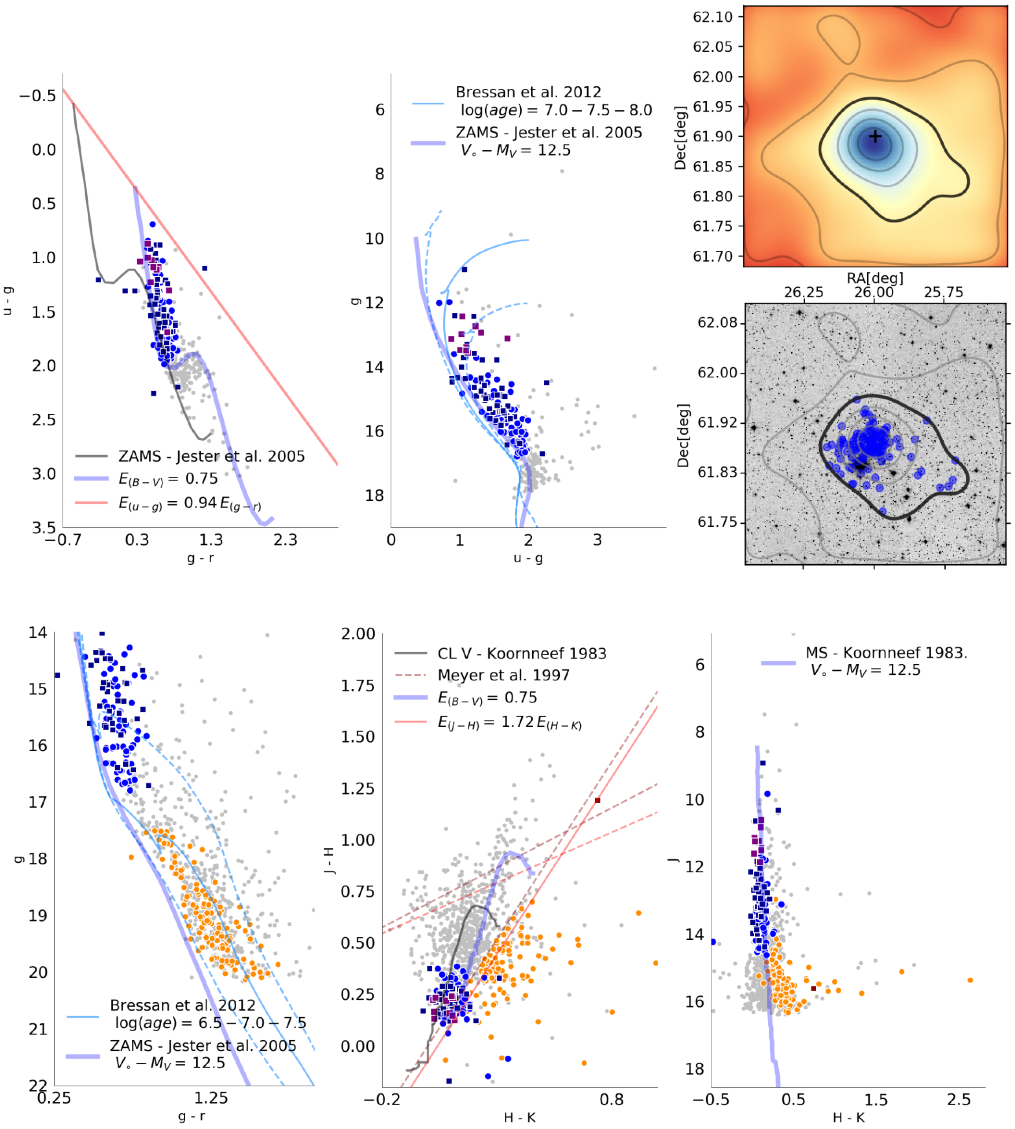

Figure 7. NGC 654. Similar description to Fig. 3. The purple squares indicate stars with ST that where used to calculate mean values for distance and colour excess.

Overdensity studies revealed a density ratio of $\rho_\circ/\rho_{\rm out} \approx 2$ and since optical SDSS images partially cover the cluster, the UMS stars are distributed outside the real region of maximum density.

Photometric diagrams are shown in Fig 5. From the locus of the three stars with spectral classification and those adopted to be UMS, we inferred a nuclear age of 3–10 Myr. On the other hand, from *Gaia* astrometric data analysis, we calculated a distance of 4.0 ± 0.6 kpc (see Fig 18). Distance modulus and $B - V$ colour excess using photometric diagrams were estimated in 12.9 (3.8 kpc) and 0.85, respectively. These values are in agreement with those calculated for the three stars with spectral classification and *Gaia* results.

4.3 NGC 659

NGC 659 is a known young star cluster, first studied by Steppe (1974) using *UGR* photometry from which they derived distances from 2.3 to 3 kpc ($V_\circ - M_V = 11.8$–12.4). Later, Phelps & Janes (1994), using CCD photometry in the *UBV* system, estimated an age of 22 Myr and placed this object at 3.5 kpc ($V_\circ - M_V = 12.7$) with an $E_{(B-V)} \approx 0.63$. Recently, Dambis et al. (2017), based on IPHAS and APASS photometric data, estimated a distance of $\sim$ 2.7 kpc ($V_\circ - M_V = 12.16$) and an $E_{(B-V)} \approx 0.74$, whereas Cantat-Gaudin et al. (2018) used *Gaia* DR2 to determine a dmode of $\sim$ 3.2 kpc. In particular, the MWSC place the cluster at 2.3 kpc ($V_\circ - M_V = 11.8$) with a colour excess of 0.95 and an age of $\sim$ 60 Myr.

Spectroscopic data were obtained from Mathew & Subramaniam (2011). They catalogued three B-type stars: two B1e V (2MASS J01442268+6040434 and 2MASS J01442808+6040033) and one B2e V (2MASS J01443316+6040564). Since SDSS photometry was saturated for both B1e V stars, we only used the B2e V star to calculate a spectrophotometric distance module of $V_\circ - M_V = 12.68$ and a colour excess of $E_{(B-V)} = 0.79$.

Our stellar overdensity analysis presented most UMS star concentrated towards the centre of the cluster. We derived a density

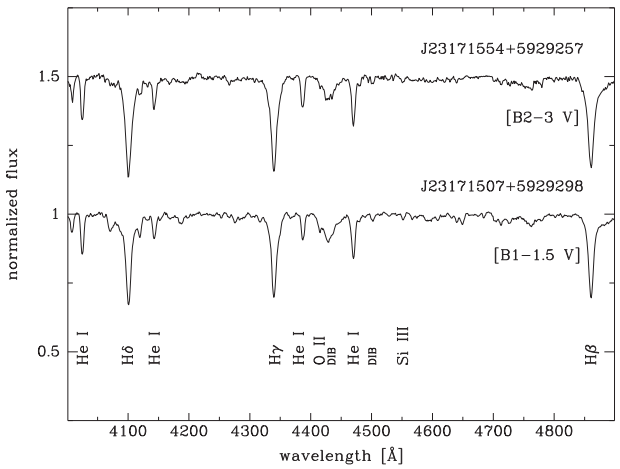

Figure 8. Optical spectra obtained for the two B-type stars in IRAS 23151+5912. Object identifications, spectral classifications, and most noticeable features are labelled.

ratio of $\rho_\circ/\rho_{\rm out} \approx 4.6$. Analysing these stars using *Gaia* DR2 we calculated a distance of 3.2 ± 0.4 kpc.

Fig. 6 shows the photometric diagrams built with stars inside the studied region, where blue circles are the UMS and dark blue squares indicate stars derived from *Gaia* analysis. We obtained a good trace of both selections of stars and we used them to estimate the cluster fundamental parameters, yielding a distance of 3.2 kpc ($V_\circ - M_V = 12.5$) and an $E_{(B-V)} = 0.80$. In particular, results for the B2 V star are in agreement with both, photometric estimations and *Gaia* data analysis results. Also IR photometric diagrams show a coherent distribution of the three stars with their ST classification, both in the TCD and in the CMD as well as all the UMS (see Fig. 6). We also estimated the nuclear age between 10 and 30 Myr and contraction age $\sim$ 10 Myr.

4.4 NGC 654

NGC 654 was studied using *UBV* photoelectric photometry by Huestamendia, del Rio & Mermilliod (1993). They found a distance modulus of $V_\circ - M_V = 12$ (2.5 kpc), a wide range in colour excess $E_{(B-V)} = 0.74$–1.19, and an age of 14 Myr. Phelps & Janes (1994) also studied this cluster using CCD photometry in the *UBV* system and derived distance, colour excess, and age of 3.5 kpc ($V_\circ - M_V = 12.15$), 0.90, and 8–25 Myr, respectively, while Dambis et al. (2017) estimated 2.5–2.7 kpc for distance ($V_\circ - M_V = 12$–12.2), $E_{(B-V)} \approx 0.8$, and an age of $\sim$30–100 Myr. The MWSC lists the following parameters for this cluster: distance $\sim$ 1.7 kpc ($V_\circ - M_V = 11.2$), $E_{(B-V)} = 0.75$, and age $\sim$ 20 Myr. Recently, Cantat-Gaudin et al. (2018) derived a distance (dmode) of 2.9 kpc using *Gaia* astrometric data.

We found 31 B-type stars in the literature in the NGC 654 region (see Table 3). Therefore, we could calculate individual spectrophotometric distances and found a significant dispersion. Taking into account, simultaneously their position in the photometric diagrams, their spectrophotometric distance, and the corresponding distance derived from *Gaia* data analysis (3.0 ± 0.3 kpc), we selected 10 of the 31 B-type stars. Thus, the computed values for the mean distance and colour excess yielded $(V_\circ - M_V) = 12.5$ (3.1 kpc) and $E_{(B-V)} = 0.9$.

We constructed stellar density maps using sources with $J < 17$ and we found an overdensity of $\rho_\circ/\rho_{\rm out} \approx 3.4$. Using stars within this selection we build the TCDs and CMDs (see Fig. 7). Distances estimated photometrically and derived from *Gaia* data analysis were of the same order (see Fig. 18). For colour excess, we estimated $E_{(B-V)} = 0.75$, slightly smaller than the spectrophotometric result. All 10 stars used for spectrophotometric calculations are shown with purple squares in Fig. 7. From isochrone fitting we derived a nuclear age of $\sim$ 30 Myr. PMS population is indicated in Fig. 7 with orange circles from which we estimated a contraction age of also 10–30 Myr.

4.5 IRAS 23151+5912

The IRAS 23151+5912 open cluster is located south-east of a molecular cloud (Rodríguez-Esnard, Migenes & Trinidad 2014) and an H II region (LBN 111.14-00.72; Dubout-Crillon 1976). It was studied by Wouterloot & Brand (1989) and Sridharan et al. (2002). They determined the kinematic distances of 5.57 and 5.7 kpc ($V_\circ - M_V = 13.7$–13.8), respectively. The cluster is included in the MWSC with a distance of 2.9 kpc ($V_\circ - M_V = 12.3$), a colour excess of 1.25, and an age of $\sim$ 200 Myr.

We selected the two brightest stars for spectroscopic observation, 2MASS J23171554+5929257 and 2MASS J23171507+5929298. Both have similar spectral characteristics as early B stars, as can be seen in the Fig. 8. A tailored analysis permits to distinguish some differences between them, i.e. in the brightest star it is possible to identify Si III, Si II, and O II lines which points to a B1-1.5 V type, while the other spectrum seems to be quite later, B2-3 V, because Mg II λ4481 and C II λ4267 are marginally detected (but not in the former). Unfortunately, both stars are saturated in the SDSS images, but J23171507+5929298 has a non-saturated entry in the APASS survey, so we estimated a distance of 2.2 kpc ($V_\circ - M_V = 12.22$) and a colour excess of 0.8.

From stellar density analysis of this region we calculated a relatively low overdensity $\rho_\circ/\rho_{\rm out} \approx 1.7$. Optical and infrared photometric diagrams (see Fig. 9) showed a small population of UMS stars, a PMS population, and a few YSO candidates. Results from *Gaia* data analysis situate this cluster at a distance of 3.2 ± 0.2 kpc (see Fig. 18). Regarding colour excess, we estimated a similar value to the calculated from the B1 V star. In spite of the low amount of UMS stars we used the B1 V to select the isochrone ($\sim$30 Myr) that represented this small clusters age. From the traces of the PMS population we estimated a contraction age similar to the nuclear age (see Table 2).

4.6 FSR 0417

FSR 0417 is presented in the MWSC as an evolved open cluster, at a distance 2.9 kpc ($V_\circ - M_V = 12.3$), an $E_{(B-V)} \approx 1.25$, and an age of $\sim$ 200 Myr. This stellar cluster was also studied by Buckner & Froebrich (2013), using an automatic method to estimate distances and reddening from near-infrared photometry alone, and obtained a distance of 3.2 kpc.

We classified the optical spectrum of 2MASS J23134725+5953568 as B1-2 V (see Fig. 10). Among the most conspicuous absorption lines used are Si III λ4552 and the C III + O II λλ4070, 4650 blends.

This cluster inhabits the H II region catalogued as LBN 110.96-00.83 (Dubout-Crillon 1976). In this particular case, overdensity maps were better achieved by using *g* optical band, with stars

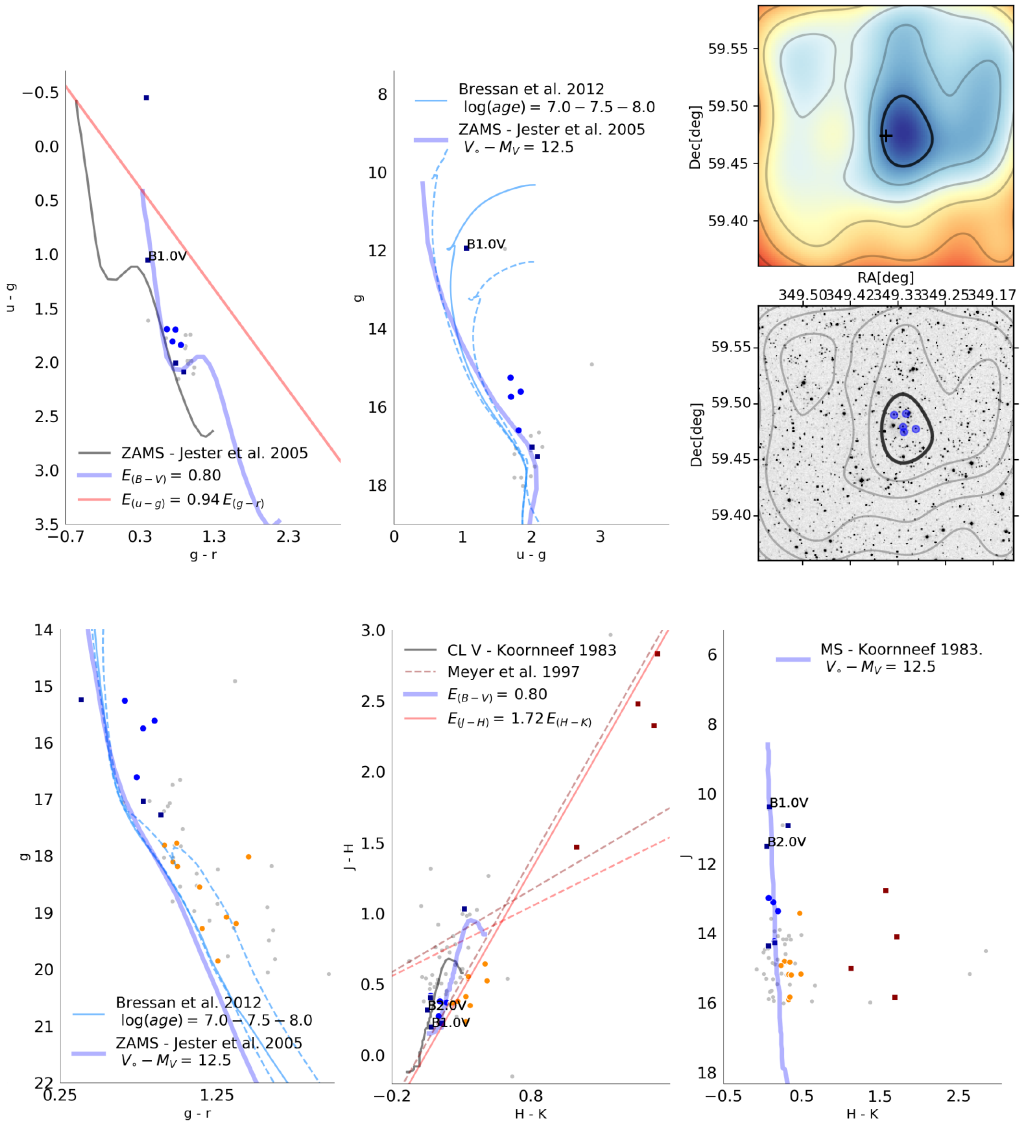

Figure 9. IRAS 23151+5912. Similar description to Fig. 3. The red squares indicate YSO candidates.

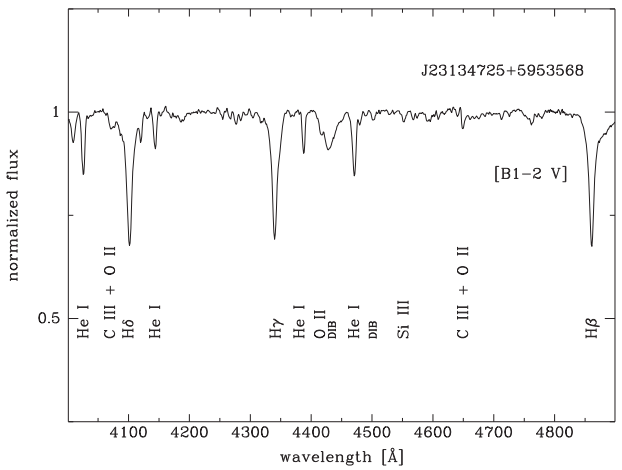

Figure 10. Optical spectra obtained for the B-type star in FSR 0417. Object identifications, spectral classifications, and most noticeable features are labelled.

brighter than $g = 18$. Photometry analysis is shown in Fig. 11. We derived a distance module $V_\circ - M_V = 12.5$ (3.2 kpc), and $E_{(B-V)} = 0.85$. Distance was estimated considering the locus of the UMS, the spectroscopic calculation, and the distance derived from *Gaia* data analysis (3.2 ± 0.5 kpc). Estimated colour excess was moderately different than the one calculated for the B1 V star but acceptable. In spite of the age listed in the MWSC, we concluded that FSR 0417 is a young star cluster, with a nuclear age of 3–10 Myr. Fig. 11 also shows a PMS population (orange circles) which suggests a contraction age of 10–30 Myr.

4.7 NGC 7510

Sagar & Griffiths (1991) studied NGC 7510 using CCD photometry *BVI* and estimated a distance module of $V_\circ - M_V = 12.5$ (3 kpc) and an $E_{(B-V)} = 1.0$–1.3. Using empirical isochrones, they established an age of ∼ 10 Myr. Barbon & Hassan (1996) found similar values, i.e. $V_\circ - M_V = 12.45$ (∼3 kpc), $E_{(B-V)} = 1.2$, and an age of ∼ 10 Myr, by means of photographic *UBV* photometry. The MWSC lists the following values for this cluster: $V_\circ - M_V = 11.6$ (2.1 kpc),

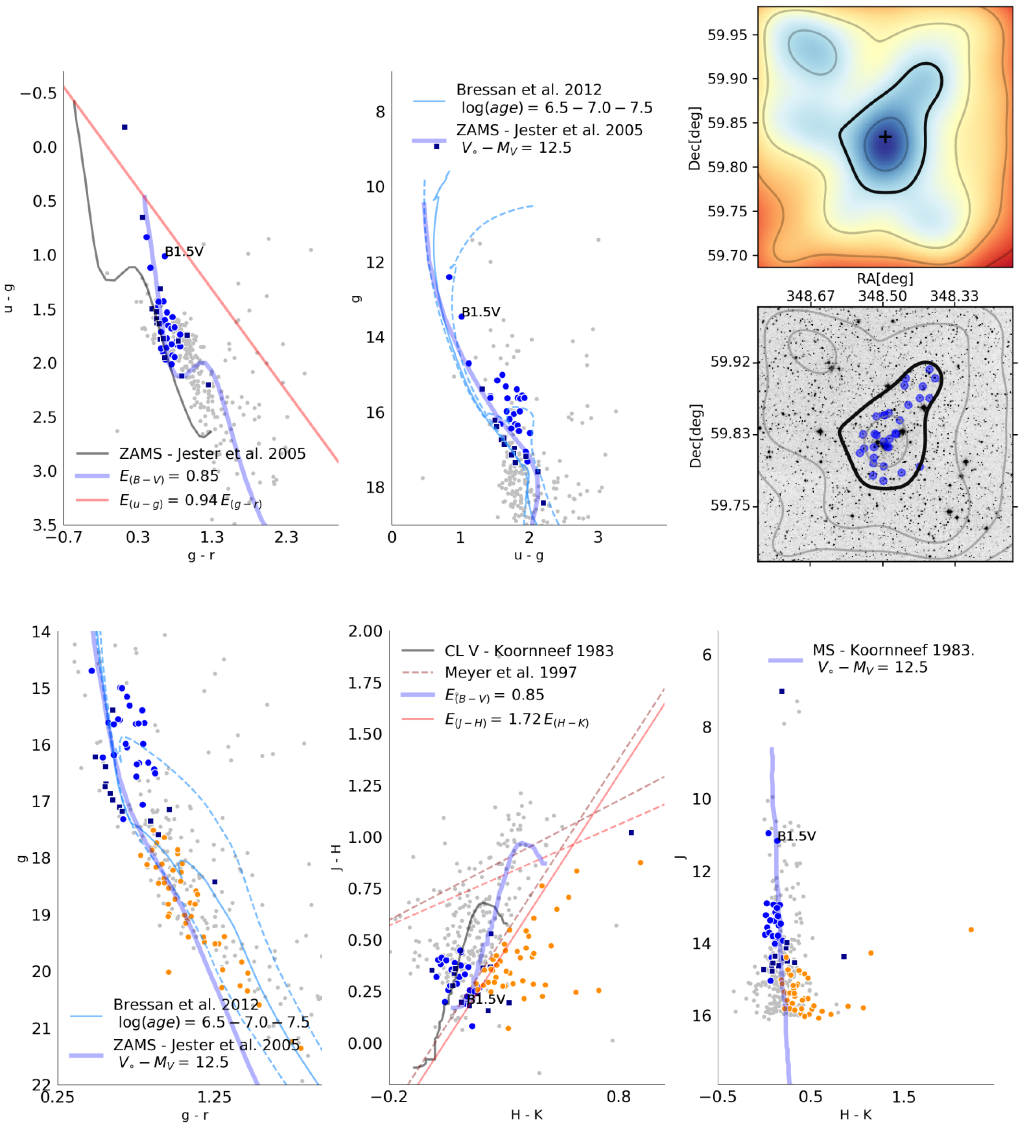

Figure 11. FSR 0417. Similar description to Fig. 3.

$E_{(B-V)} = 0.95$, and an age $\sim$ 50 Myr. From *Gaia* DR2 analysis, Cantat-Gaudin et al. (2018) calculated for this cluster a dmode of 3.2 kpc.

The stellar density map analysis showed a clear overdensity revealing a very populated open cluster, with a density ratio of $\rho_\circ/\rho_{\rm out} \approx 5.9$. UMS stars are situated very close to the clusters centre, as shown in Fig. 12. This cluster presents a young population of B-type stars. B1e V star was not considered as it is saturated in SDSS images and no other fluxes were found in other data bases. We used the remaining four for calculating mean values of distance $\sim$ 1.1 kpc ($V_\circ - M_V = 10.5$) and colour excess $\sim$ 1.1 (see Table 3).

Photometric diagrams of this region showed a cluster that appears to be very contaminated by field stars. For this purpose we relied in our distance provided by *Gaia* data analysis (3.2 $\pm$ 0.5 kpc). Besides the best fit of the ZAMS suggested an almost similar distance as the just mentioned. Also the same colour excess but a greater distance than the calculated with spectral information. We established a distance of $\sim$ 3.1 kpc ($V_\circ - M_V = 12.5$) and a colour excess $E_{(B-V)} = 1$. Contraction age was estimated in $\sim$ 10 Myr from the PMS population distribution and nuclear age between 10 and 30 Myr. Discrepancies in distance when comparing photometric estimations with spectrophotometric calculation were also found by Barbon & Hassan (1996) i.e. they determined a distance modulus 1.75 mag greater than the one derived from spectral data. This difference was explained by evolutionary effects of the most massive star.

4.8 [BDS2003] 39

[BDS2003] 39 is a small open cluster catalogued by Bica et al. (2003) and embedded in the compact IC 1470 H II region (Dubout-Crillon 1976) not listed in the MWSC. Israel, Habing & de Jong (1973) conducted observations at 21 cm of this region and established a distance of 3.5 kpc. Lynds & Oneil (1983) studied IC 1470 and proposed that the H II region was excited by a single O7 ST star. Russeil, Adami & Georgelin (2007) concluded that the ST of the exciting star of this region was a O8 V star and established a distance or $\sim$ 2.38 kpc.

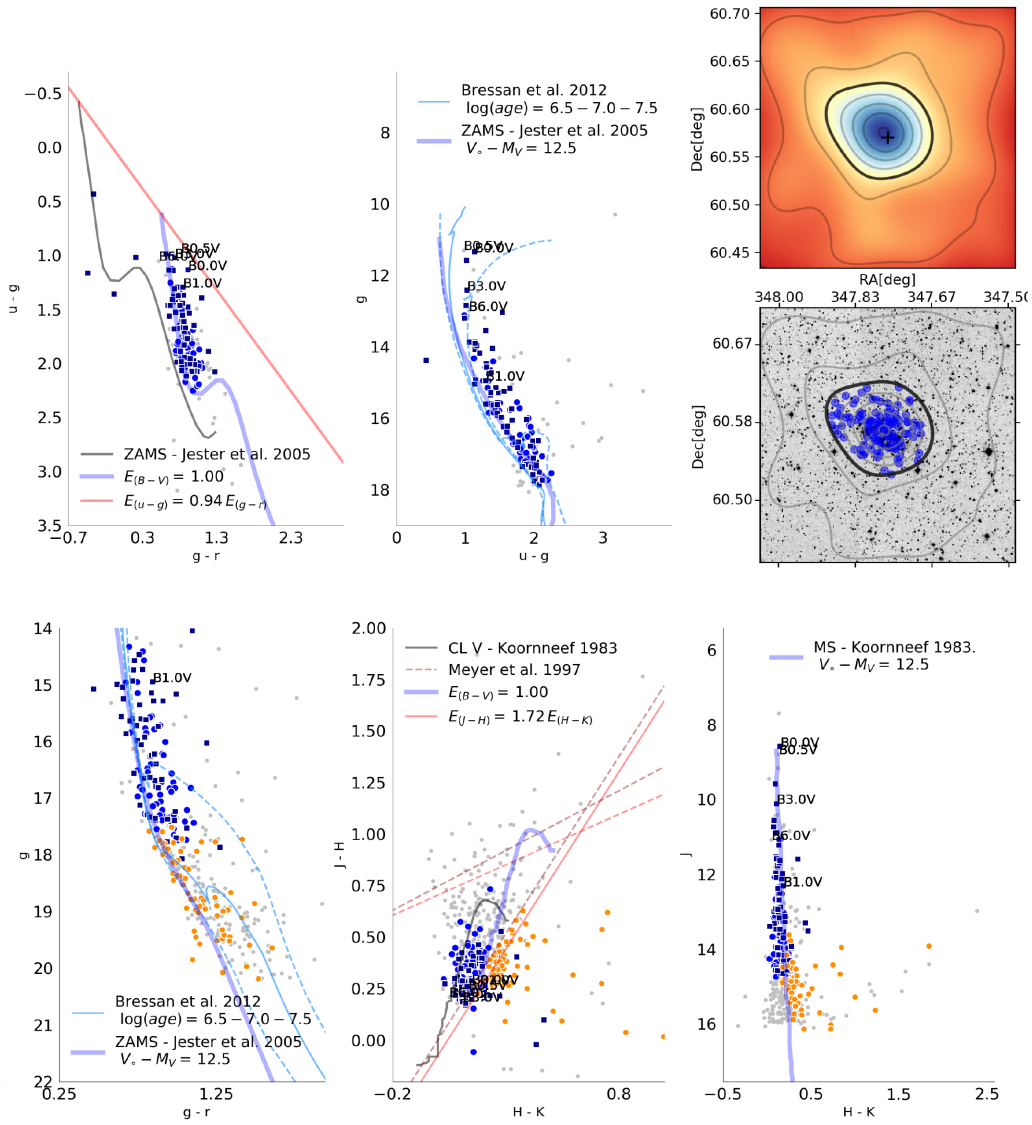

Figure 12. NGC 7510. Similar description to Fig. 3.

Ratio of densities for this region was calculated in $\rho_\circ/\rho_{\rm out} \approx 6$. This represents clear overdensities with few UMS stars situated at the very centre of the H II region. Fig. 13 shows the density maps and the optical TCD and CMD. For spectrophotometric analysis we adopted the O8 V star, determined by Russeil et al. (2007), and calculated a spectrophotometric distance module of 11.23 (1.8 kpc) and a colour excess of 1.75. We used similar values for photometric analysis, and found a very good agreement. The optical TCD shows a significant dispersion of the UMS towards more reddening values. This differential reddening is because the clusters are embedded in the compact IC 1470 H II region. In turn, high reddening values of the O8 V star is revealed by its locus on 2MASS TCD. Regarding the cluster state of evolution, we established a nuclear age of 1–3 Myr.

4.9 BFS 16

This small group of stars is situated at the centre of the H II region BFS 16 and has not been identified as a star cluster. The H II region was studied by Fich & Blitz (1984) where they obtained a kinematic distance of ∼ 4.8 kpc, while Russeil et al. (2007) calculated a Galactocentric distance of 9.9 kpc, adopting for the Sun a Galactocentric distance of 8.5 kpc.

Our spectroscopic observations revealed that 2MASS J23035125+6024163 is a B3-4 V star (Fig. 14). This spectral classification was inferred from the presence of lines from low ionized ions, i.e. Si II λ4128, C II λ4267, and Mg II λ4481, and the strong He I lines. Adopting a B3 V ST we calculated a distance of 2.3 kpc ($V_\circ - M_V = 11.8$) and a colour excess of 1.1.

Stellar overdensity analysis revealed a clear overdensity, i.e. a relation of $\rho_\circ/\rho_{\rm out} \approx 5$. The few UMS stars of this cluster, shown in Fig. 15, are situated relatively close to the central region, ionizing the molecular gas cloud. Our photometric analysis (see Fig. 15) indicated for this cluster a distance module of $V_\circ - M_V = 11.8$ (2.3 kpc) and a colour excess of 1.1, same as the ones derived from spectral data. We estimated for this young embedded stellar clusters a nuclear age of 3–10 Myr.

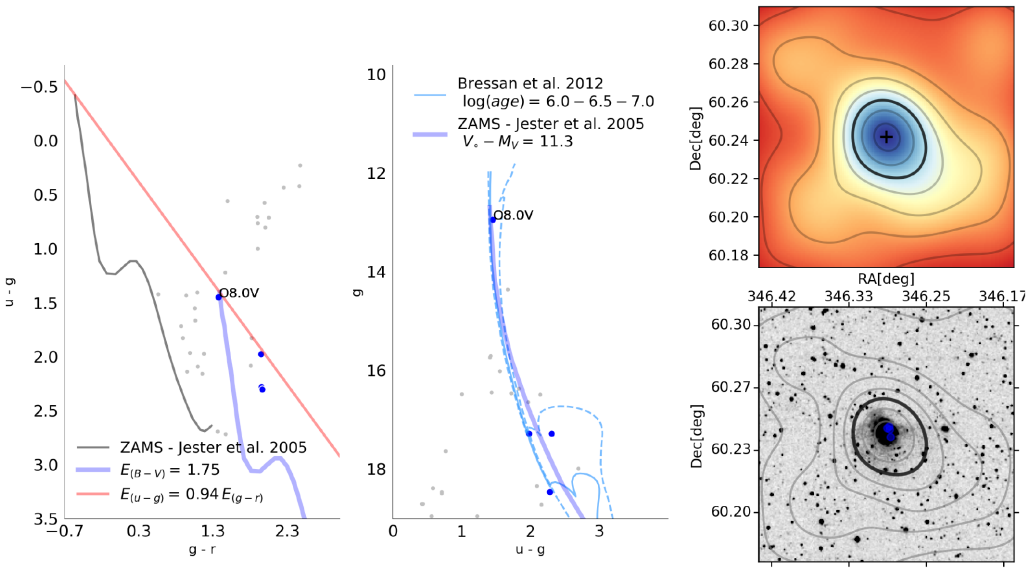

Figure 13. [BDS2003] 39. Similar description to Fig. 3.

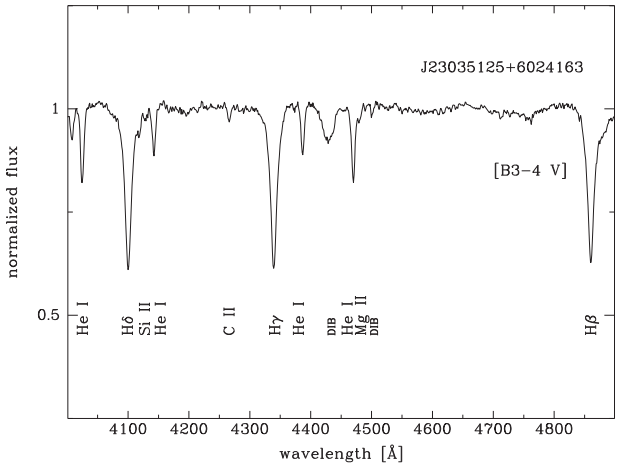

Figure 14. Optical spectra obtained for the B-type star in BFS 16. Object identifications, spectral classifications, and most noticeable features are labelled.

4.10 Kronberger 80

Open cluster Kronberger 80 is situated in the vicinity of the ionized H II region GAL 093.06+02.81 (Lockman 1989). The MWSC lists this compact object as an evolved star cluster (∼ 550 Myr) situated at a distance of ∼ 5 kpc ($V_\circ - M_V = 13.5$), with a colour excess of ∼ 1.3. This cluster was located by Cantat-Gaudin et al. (2018) at 10 kpc (dmode) using *Gaia* DR2.

We calculated a density ratio of $\rho_\circ/\rho_{\rm out} \approx 5$, with UMS stars at its centre and also widely distributed along the studied region. Photometry data analysis shown in Fig. 16 presents this UMS well defined in the optical TCD and CMD. Regarding the *JHK* TCD it can be distinguished that two of the UMS stars (blue circles) are widely scattered, while a handful inhabits the region of early-type stars. Taking all this into account we were able to estimate the clusters distance module $V_\circ - M_V = 14.2$ (7 kpc), and colour excess 2.6. From isochrone fitting, also shown in Fig. 16, it seems clear that this is a young open cluster with an age of no more than 30 Myr.

5 DISCUSSION

In our previous work (Molina Lera et al. 2018) we revealed that several clusters considered belonging to the 'Perseus Arm' are in fact located in a scatter way covering more than a single spiral arm. In particular, clusters [BDS2003] 42, Mayer 2, and probably Kronberger 80 belong to the 'Outer Arm', and clusters Teutsch 45 and Juchert 19 can be associated with a more external inter-arm feature or even the 'New Arm' identified by Sun et al. (2015) using H I and CO data. In this work, we verified the previous estimated distance and youth for Teutsch 45 by using spectroscopic classification of two early stars (see Table 3) in this region. We also conducted an analysis to six of the 10 clusters regions using *Gaia* DR2 and derived independent distance calculations from those ones using spectral and photometric information. Considering our previous paper and the present one, we confirmed the photometric-based methodology to estimate the distances to young clusters; we re-enforced the idea concerning to the presence of a young populations located at the 'Outer Arm' in the 2GQ, and we provided more evidence of the presence of the 'New Arm'.

In the cases of the most studied clusters, we found similar results to those ones previously published, and for the objects that were only identified or that had been poorly studied, we established new or unpublished parameters. In relation to different R_V values, we found that for $R_V = 3.4$ distances decrease in their values up to 10 per cent, while for $R_V = 2.9$ they increase up to 5 per cent. Variations in colour excess were not significant. These results lead to remark that $R_V = 3.4$ places Teutsch 45 close to the 'New Arm', whereas nearby clusters would not significantly modify their location.

Regarding the Galactic structure at the 2GQ, we present in Fig. 17 the resulting picture according to our results found in this work and those already given by Molina Lera et al. (2018). They were put together to the spiral pattern provided by Hou & Han (2014) and extending the 'New Arm' path into the 2GQ. We noticed that most of the clusters studied in this work are located in the 'Perseus/Orion Arm' with the exception of Waterloo 1 and Teutsch 45. In particular, a trace from NGC 7510/FSR 0417 to Waterloo 1 with other four clusters between them consistent with the location of several H II regions could be noticed. This path could be representative of an

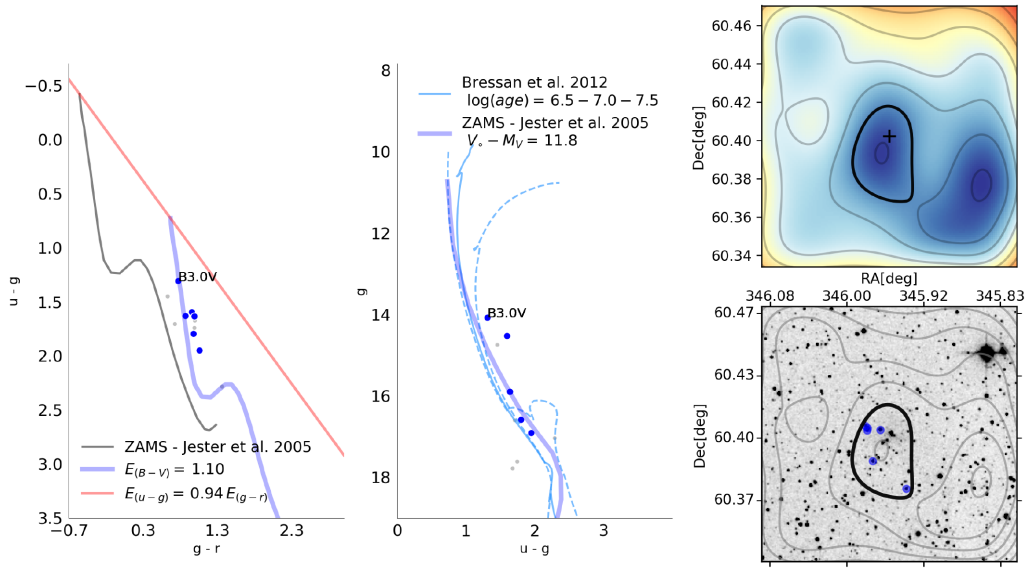

Figure 15. BFS 16. Similar description to Fig. 3.

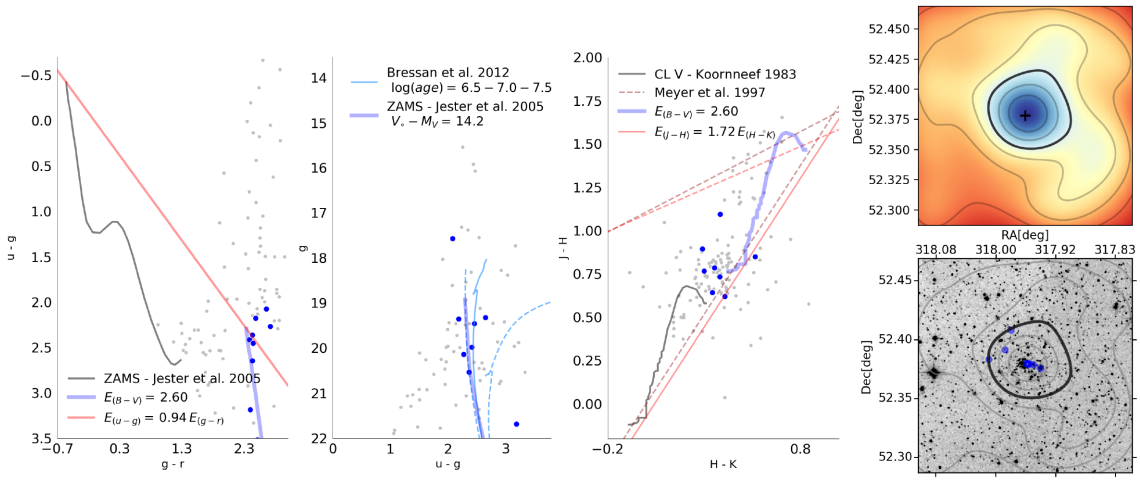

Figure 16. Kronberger 80. Similar description to Fig. 3.

inter-arm feature. This kind of structure are commonly observed in several spiral galaxies and seem to be caused by sheared structures from the main arms as a consequence of divergent orbits or differential compression of gas in spiral galaxies (Dobbs & Bonnell 2006, Shetty & Ostriker 2006). Regarding Kronberger 80 results given by Cantat-Gaudin et al. (2018) situates this cluster at a distance of 10 kpc which locates it right in the 'Outer arm'. This distance cannot be totally discarded considering $R_V = 3.4$ and taking into account that photometric values for this cluster present high errors.

6 CONCLUSIONS

We presented a study of a second selection of young clusters along the Galactic plane in the 2GQ. This analysis included multiband photometric data complemented with new spectroscopic observations and available information in the literature. We also conducted an analysis of distance using *Gaia* DR2. Thus, we were able to determine the clusters main parameters. In particular, we confirmed their youth by the identification of early-type stars among their members. On the other hand, we completed our previous study (Molina Lera et al. 2018) to better trace the structure of the Milky Way in the 2GQ.

Concerning the particularities of each studied cluster, it is possible to list the following remarks:

(i) Teutsch 45: Our spectroscopic information and spectrophotometric calculation confirmed our previews results, i.e. a young open cluster, situated at a distance of ~ 8 kpc further away than previews estimations.

(ii) Waterloo 1: Our estimated colour excess ($E_{(B-V)} = 0.85$) and distance (3.8 kpc) were similar to the one presented by Moffat et al. (1979), and *Gaia* data analysis results were also in agreement with Cantat-Gaudin et al. (2018). Regarding age, the MWSC lists an age of 400 Myr, while in this work we established a nuclear age (3–10 Myr), in agreement with its early-type stars population.

(iii) NGC 659: Our study regarding distance is similar to Phelps & Janes (1994) ($\sim$ 3.2 kpc) and to Cantat-Gaudin et al. (2018). Colour excess was similar to that listed in the MWSC i.e. $\sim 0.75 \pm 0.15$. As for nuclear age, we estimated 10–30 Myr and a

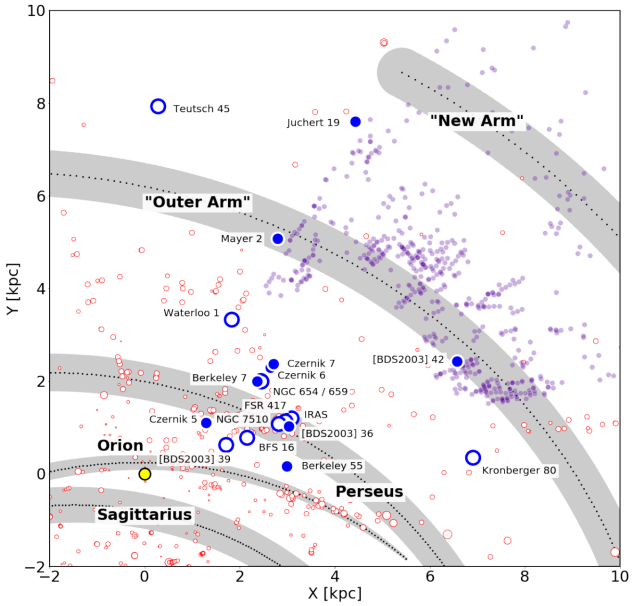

Figure 17. Studied clusters projected in the Galactic plane with the HH2014 (Hou & Han 2014) model with four logarithmic spiral arms. The figure covers mainly the 2GQ. The yellow circle marks the position of the Sun and we assumed a distance to the Galactic Centre of $R_{\odot} = 8.5$ kpc. The large filled (blue) circles indicate the selected clusters studied by Molina Lera et al. (2018), whereas hollow ones correspond to those studied in this work. Other arm tracers are plotted for reference: open (red) circles are H II regions HH2014 (Hou & Han 2014) and filled (violet) small circles are molecular clouds detected with CO observations (Dame & Thaddeus 2011; Sun et al. 2015; Du et al. 2016). IRAS 23151+5912, FSR 0417, and NGC 7510 locations were slightly displaced for clarity.

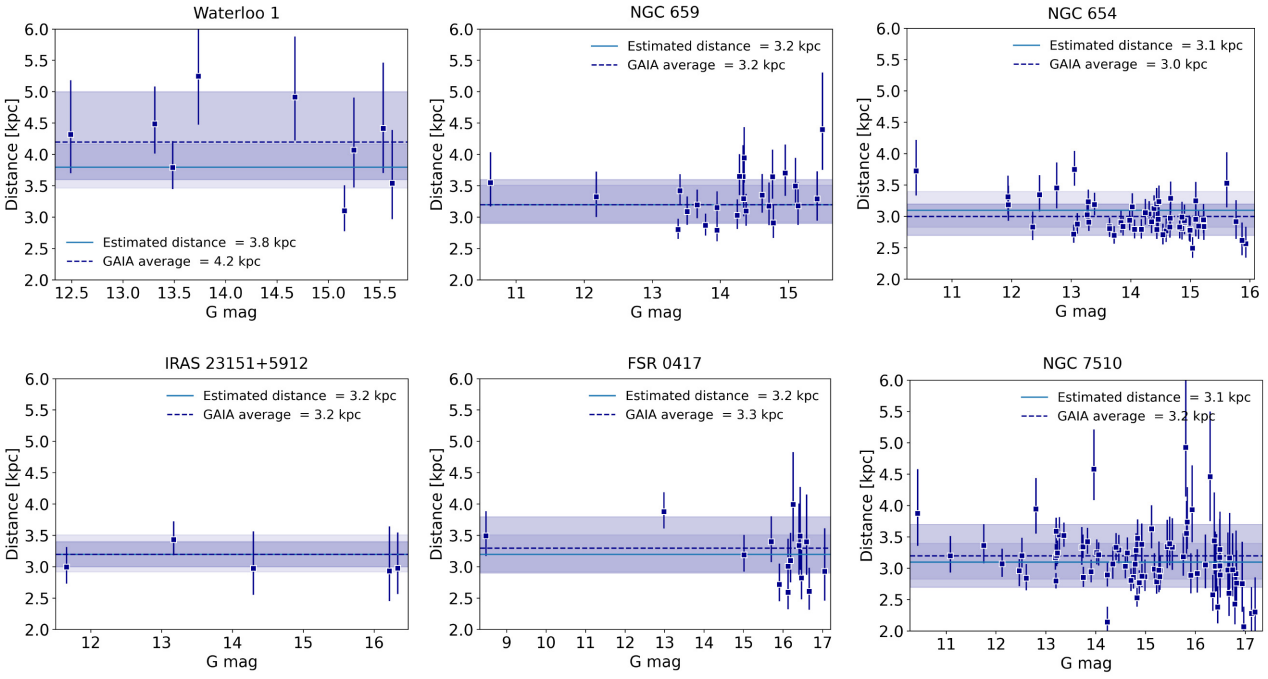

Figure 18. Distance versus G mag. (*Gaia* magnitude filters). The dashed dark blue line corresponds to the weighted average distance calculated with stars and their errors indicated with dark blue squares and vertical lines, respectively. The blue line indicates distances from Table 2. The blue shadows surrounding each line corresponds to each calculated error.

contraction age of ∼ 10 Myr, which is consistent with the B-type star population established from spectroscopic information.

(iv) NGC 654: Our distance and colour excess (∼ 3.1 kpc and $E_{(B-V)} = 0.75$) was similar as the one estimated by Phelps & Janes (1994) and calculated by Cantat-Gaudin et al. (2018). Nuclear age, estimated in ∼ 30 Myr and contraction age between 10 and 30 Myr are of the order of the MWSC (20 Myr).

(v) IRAS 23151+5912: We found equal values regarding nuclear and contraction ages (∼ 30 Myr). These results differ significantly from that catalogued by the MWSC (∼ 200 Myr). It should be

Table 3. Main parameters for stars with ST.

Source	2MASS/id	$\alpha_{J2000.0}$	$\delta_{J2000.0}$	ST	$ST_{adopted}$	M_V	$E_{(B-V)}$	$V_\circ - M_V$
			Teutsch 45					
TW*	05424388+3058051	5:42:43.9	30:58:05.0	B0.5-1V	B0.5V	−3.52	0.98	14.29
TW*	05424991+3056454	5:42:49.9	30:56:45.4	B1-2V	B1.0V	−3.20	1.03	14.85
			Waterloo 1					
TW*	04183563+5251541	4:18:35.6	52:51:54.2	O8-8.5V	O8.0V	−4.70	0.83	13.08
SB*	04183950+5250550	4:18:39.5	52:50:55.1	B1.5V	B1.5V	−2.85	0.83	12.85
TW*	04183481+5251575	4:18:34.8	52:51:57.6	B2-3V	B2.0V	−2.50	1.07	12.92
			NGC 659					
M&S	J01442268+6040434	1:44:22.7	60:40:43.5	B1Ve	B1.0V	−3.20	–	–
M&S	J01442808+6040033	1:44:28.1	60:40:03.3	B1Ve	B1.0V	−3.20	–	–
M&S*	J01443316+6040564	1:44:33.2	60:40:56.5	B2Ve	B2.0V	−2.50	0.79	12.68
			NGC 654					
SB*	J01434647+6152515	1:43:46.5	61:52:51.6	B1V	B1.0V	−3.20	0.91	12.74
SB	J01440191+6153251	1:44:01.9	61:53:25.2	B1V	B1.0V	−3.20	1.52	9.85
SB*	J01440189+6155168	1:44:01.9	61:55:16.8	B1V	B1.0V	−3.20	1.13	12.10
SB*	J01435915+6155187	1:43:59.1	61:55:18.7	B1V	B1.0V	−3.20	1.11	12.36
SB	J01430402+6148356	1:43:04.0	61:48:35.5	B1.5Ie	B1.5I	−6.50	0.84	15.52
SB*	J01435113+6154258	1:43:51.2	61:54:25.9	B1.5V	B1.5V	−2.85	0.99	12.74
SB*	J01442096+6150374	1:44:21.0	61:50:37.5	B1.5V	B1.5V	−2.85	0.77	12.62
SB	J01441216+6152429	1:44:12.2	61:52:42.9	B1.5V	B1.5V	−2.85	0.89	13.45
SB	J01440148+6154017	1:44:01.5	61:54:01.3	B1.5V	B1.5V	−2.85	0.99	13.03
SB	J01435723+6152413	1:43:57.4	61:52:41.3	B1.5V	B1.5V	−2.85	0.86	11.82
SB	J01440803+6153429	1:44:08.0	61:53:42.9	B2II	B2.0III	−3.60	0.92	11.31
SB*	J01435182+6154194	1:43:51.9	61:54:19.4	B2V	B2.0V	−2.50	0.95	12.70
SB*	J01441776+6153153	1:44:17.8	61:53:15.2	B2V	B2.0V	−2.50	0.84	12.68
SB	J01435781+6153519	1:43:57.9	61:53:52.1	B2IV	B2.0V	−2.50	0.88	11.81
SB	J01440094+6152012	1:44:00.9	61:52:01.2	B2V	B2.0V	−2.50	0.94	13.18
SB*	J01440667+6153225	1:44:06.7	61:53:22.6	B2V	B2.0V	−2.50	0.89	12.35
SB	J01440240+6153300	1:44:02.4	61:53:30.1	B2V	B2.0V	−2.50	0.96	11.52
SB*	J01435570+6153411	1:43:55.8	61:53:41.1	B2V	B2.0V	−2.50	0.90	12.81
SB	J01440202+6153557	1:44:02.0	61:53:55.8	B2V	B2.0V	−2.50	1.53	10.20
SB	J01440073+6153517	1:44:00.7	61:53:51.8	B2V	B2.0V	−2.50	0.88	13.98
SB	J01435543+6148332	1:43:55.4	61:48:33.3	B2V	B2.0V	−2.50	0.83	13.19
SB	J01435774+6154017	1:43:57.7	61:54:01.8	B2.5V	B2.5V	−2.10	1.05	11.96
SB	J01441177+6153593	1:44:11.8	61:53:59.1	B2.5V	B2.5V	−2.10	0.92	13.16
SB*	J01434699+6151407	1:43:47.0	61:51:40.8	B3V	B3.0V	−1.70	0.81	12.32
SB	J01442718+6153267	1:44:27.2	61:53:25.8	B3V	B3.0V	−1.70	0.97	11.95
SB	J01440419+6153559	1:44:04.3	61:53:56.1	B3V	B3.0V	−1.70	1.01	13.29
SB	J01435196+6153586	1:43:52.0	61:53:59.4	B3V	B3.0V	−1.70	1.18	10.44
SB	J01435338+6153121	1:43:53.4	61:53:12.2	B4V	B4.0V	−1.25	0.20	14.32
SB	J01441310+6152309	1:44:13.1	61:52:31.2	B5V	B5.0V	−1.00	0.72	10.06
SB	J01442173+6151438	1:44:21.7	61:51:43.8	B6V	B6.0V	−0.70	0.66	10.38
SB	J01435144+6151111	1:43:51.4	61:51:11.2	B6V	B6.0V	−0.70	0.80	9.55
			IRAS 23151+5912					
TW	J23171554+5929257	23:17:15.5	59:29:25.4	B2-3V	B2.0V	−2.50	–	–
TW*	J23171507+5929298	23:17:15.2	59:29:29.1	B1-1.5V	B1.0V	−3.20	0.84	12.22
			FSR 0417					
TW*	J23134725+5953568	23:13:47.3	59:53:56.9	B1-2V	B1.5V	−3.20	1.05	12.55
			NGC 7510					
SB	J23105736+6034015	23:10:57.4	60:34:01.4	B0Ve	B0.0V	−3.85	1.32	10.45
SB	J23110287+6033327	23:11:02.9	60:33:32.8	B0.5V	B0.5V	−3.52	1.22	10.44
SB	J23110853+6035032	23:11:08.5	60:35:03.3	B1Ve	B1.0V	−3.20	–	–
SB	J23105917+6033184	23:10:59.2	60:33:18.5	B3V	B3.0V	−1.70	1.07	10.26
SB	23110544+6035075	23:11:05.4	60:35:07.6	B6V	B6.0V	−0.70	0.81	10.81
			[BDS2003] 39					
R*	J23051015+6014427	23:05:10.1	60:14:42.7	O8V	O8.0V	−4.70	1.75	11.23
			BFS 16					
TW*	23035125+6024163	23:03:51.2	60:24:16.0	B3-4V	B3.0V	−1.70	1.10	11.80

Note: TW: This Work. SB: *SIMBAD*. M&S: Mathew & Subramaniam (2011). R: Russeil et al. (2007). (*) indicates stars used to estimate clusters parameters.

noted that our results are consistent with the population of B-type star derived from our spectroscopic campaign. We also found traces of YSO candidates. Regarding distance we established that this cluster is much closer than previewers studies, from 5.57 and 5.7 kpc (Wouterloot & Brand 1989 and Sridharan et al. 2002, respectively) to 3.2 kpc. Reddening values also showed significant differences; we estimated a colour excess of 0.80, while the MWSC listed 1.25.

(vi) FSR 0417: We found differences in comparison with previews works. We established that this is a young star cluster with at least a B-type star ($\sim$ 30 Myr), unlike the MWSC which listed an age of $\sim$ 200 Myr. We estimated a distance and a reddening of 3.2 kpc and $\sim$ 0.85, respectively, while the MWSC and Buckner & Froebrich (2013) established 2.9 kpc and an $E_{(B-V)} \approx 1.25$.

(vii) NGC 7510: We found similar values for distance (3.1 kpc) and colour excess (1.0) as previews works (Sagar & Griffiths 1991 and Barbon & Hassan 1996). *Gaia* data analysis was also in agreement with Cantat-Gaudin et al. (2018). The MWSC lists a distance much smaller (2.1 kpc). On the other hand we estimated nuclear and contraction ages of 10–30 and $\sim$ 10 Myr, respectively.

(viii) [BDS2003] 39: Our calculated distance (1.8 kpc) for this cluster situates it much closer than previews works (3.5 and 2.38 kpc). We also estimated a nuclear age of 1–3 Myr.

(ix) BFS 16: We detected a B3-4 V star, from which we calculated a distance of 2.3 kpc and a colour excess of 1.1. Same results were found from photometric data analysis. We also established a nuclear age of 3–10 Myr. These are the first parameters derived for this open cluster.

(x) Kronberger 80: Our results are different from that listed in the MWSC and Cantat-Gaudin et al. (2018). We estimated a distance of 7.0 kpc, a colour excess 2.6 and an age of no more than 30 Myr. While the MWSC established an age of $\sim$ 550 Myr, a distance of $\sim$ 5 kpc, with a colour excess of $\sim$ 1.3. On the other hand Cantat-Gaudin et al. (2018) derived a distance (dmode) of 10 kpc.

Looking at the global scenario, taking into account our previous paper and this one, we completed a study involving 19 open/embedded clusters located along the Galactic plane in the 2GQ. All of them were analysed with a systematic and homogeneous method that involves the same set of tools applied to data of the same nature (photometric surveys and spectroscopic observations). This procedure minimizes bias in the results. Most of the clusters were useful for describing the Galactic disc structure in the 2GQ. They allow us to better trace the 'Outer Arm' and suggest the presence of the 'New Arm' based on optical data. In this work, additionally and based on our spectroscopic observations, we identified seven new MS massive stars earlier than B4-type and confirmed one to be an O8-8.5. For two of the studied clusters in this paper (FRS 0417 and IRAS 23151+5912), we obtained novel *Gaia* derived distances. In nine of all studied clusters, five presented in this last work, we identified PMS population and in all of these cases we found similar values for nuclear and contraction ages, suggesting a coeval star formation process, where two of them presented YSOs candidates that should be analysed in more detail with future spectroscopic follow-up observations.

ACKNOWLEDGEMENTS

AML and GB acknowledge support from CONICET (PIP 112-201101-00301). This paper is based on observations obtained at the Gemini Observatory, which is operated by the Association of Universities for Research in Astronomy, Inc., under a cooperative agreement with the NSF on behalf of the Gemini partnership: the National Science Foundation (United States), the National Research Council (Canada), CONICYT (Chile), the Australian Research Council (Australia), Ministério da Ciência, Tecnología e Inovação (Brazil) and Ministério de Ciencia, Tecnología e Innovacíon Productiva (Argentina). This publication also used data from: (a) the Two Micron All-Sky Survey, which is a joint project of the University of Massachusetts and the Infrared Processing and Analysis centre/California Institute of Technology, funded by the National Aeronautics and Space Administration and the National Science Foundation; (b) the Wide-field Infrared Survey Explorer, which is a joint project of the University of California, Los Angeles, and the Jet Propulsion Laboratory/California Institute of Technology, funded by the National Aeronautics and Space Administration; (c) data from the ESA mission *Gaia*, processed by the *Gaia* DPAC. Funding for the DPAC has been provided by national institutions, in particular the institutions participating in the *Gaia* Multilateral Agreement. This research has also used NASA's Astrophysics Data System and the SIMBAD data base, operated at CDS, Strasbourg, France. We also wish to thank our referee Dr. Christian Moni Bidin for the suggestions and comments, which improved the original version of this work.

REFERENCES

Abreu-Vicente J., Ragan S., Kainulainen J., Henning T., Beuther H., Johnston K., 2016, A&A, 590, A131
Ahn C. P. et al., 2012, ApJS, 203, 21
Alam S. et al., 2015, ApJS, 219, 12
Bailer-Jones C. A. L., 2015, PASP, 127, 994
Barbon R., Hassan S. M., 1996, A&AS, 115, 325
Baume G., Carraro G., Comeron F., de Elía G. C., 2011, A&A, 531, A73
Benjamin R. A. et al., 2005, ApJ, 630, L149
Bica E., Dutra C. M., Soares J., Barbuy B., 2003, A&A, 404, 223
Bonatto C., Bica E., 2010, A&A, 521, A74
Bressan A., Marigo P., Girardi L., Salasnich B., Dal Cero C., Rubele S., Nanni A., 2012, MNRAS, 427, 127
Brown A. G. A. et al., 2018, A&A, 616, A1
Buckner A. S. M., Froebrich D., 2013, MNRAS, 436, 1465
Camargo D., Bonatto C., Bica E., 2015, MNRAS, 450, 4150
Cantat-Gaudin T. et al., 2018, A&A, 618, A93
Cardelli J. A., Clayton G. C., Mathis J. S., 1989, ApJ, 345, 245
Carraro G., 2014, in Feltzing S., Zhao G., Walton N. A., Whitelock P., eds, Proc. IAU Symp. 298, Setting the scene for Gaia and LAMOST. Kluwer, Dordrecht, p. 7
Carraro G., Turner D. G., Majaess D. J., Baume G. L., Gamen R., Molina Lera J. A., 2017, AJ, 153, 156
Dambis A. K., Glushkova E. V., Berdnikov L. N., Joshi Y. C., Pandey A. K., 2017, MNRAS, 465, 1505
Dame T. M., Thaddeus P., 2011, ApJ, 734, L24
Dobbs C. L., Bonnell I. A., 2006, MNRAS, 367, 873
Dubout-Crillon R., 1976, A&AS, 25, 25
Du X., Xu Y., Yang J., Sun Y., Li F., Zhang S., Zhou X., 2016, ApJS, 224, 7
Elmegreen D. M., 1980, ApJ, 242, 528
Fich M., Blitz L., 1984, ApJ, 279, 125
Gaia Collaboration, 2016, A&A, 595, A1
Grosbøl P., Carraro G., 2018, A&A, 619, A50
Henden A. A., Levine S., Terrell D., Smith T. C., Levine S., 2015, AAS, 336.16
Hou L. G., Han J. L., 2014, A&A, 569, A125
Huestamendia G., del Rio G., Mermilliod J.-C., 1993, A&AS, 100, 25
Israel F. P., Habing H. J., de Jong T., 1973, A&A, 27, 143
Kharchenko N. V., Piskunov A. E., Schilbach E., Röser S., Scholz R.-D., 2013, A&A, 558, A53
Lockman F. J., 1989, ApJS, 71, 469
Lynds B. T., Oneil E. J., 1983, ApJ, 265, 803

Mathew B., Subramaniam A., 2011, Bull. Astron. Soc. India, 39, 517
Maíz Apellániz J. et al., 2016, ApJS, 22, 4
Meyer M. R., Calvet N., Hillenbrand L. A., 1997, AJ, 114, 288
Moffat A. F. J., Fitzgerald M. P., Jackson P. D., 1979, A&AS, 38, 197
Molina-Lera J. A., Baume G., Gamen R., Costa E., Carraro G., 2016, A&A, 592, A149
Molina Lera J. A., Baume G., Gamen R., 2018, MNRAS, 480, 2386
Phelps R. L., Janes K. A., 1994, ApJS, 90, 31
Rodríguez-Esnard T., Migenes V., Trinidad M. A., 2014, ApJ, 788, 176
Russeil D., Adami C., Georgelin Y. M., 2007, A&A, 470, 161
Sagar R., Griffiths W. K., 1991, MNRAS, 250, 683
Shetty R., Ostriker E. C., 2006, ApJ, 647, 997
Sota A., Maíz Apellániz J., Morrell N. I., Barbá R. H., Walborn N. R., Gamen R. C., Arias J. I., Alfaro E. J., 2014, ApJS, 211, 10
Sota A., Maíz Apellániz J., Walborn N. R., Alfaro E. J., Barbá R. H., Morrell N. I., Gamen R. C., Arias J. I., 2011, ApJS, 193, 24
Sridharan T. K., Beuther H., Schilke P., Menten K. M., Wyrowski F., 2002, ApJ, 566, 931
Steppe H., 1974, A&AS, 15, 91
Stetson P. B., 1987, PASP, 99, 191
Stetson P. B., 1992, in Worrall D. M., Biemesderfer C., Barnes J., eds, ASP Conf. Ser., Vol. 25, Astronomical Data Analysis Software and Systems I. Astron. Soc. Pac., San Francisco, p. 297
Stoughton C. et al., 2002, AJ, 123, 485
Strutskiw M. F. et al., 2006, AJ, 131, 1163
Sung H., Lim B., Bessell M. S., Kim J. S., Hur H., Chun M.-Y., Park B.-G., 2013, J. Korean Astron. Soc., 46, 103
Sun Y., Xu Y., Yang J., Li F.-C., Du X.-Y., Zhang S.-B., Zhou X., 2015, ApJ, 798, L27
Vallée J. P., 2017, Astron. Rev., 13, 113
Walborn N. R., Fitzpatrick E. L., 1990, PASP, 102, 379
Wouterloot J. G. A., Brand J., 1989, A&AS, 80, 149
Wright E. L. et al., 2010, AJ, 140, 1868

SUPPORTING INFORMATION

Supplementary data are available at *MNRAS* online.

Supplementary Tables.

Please note: Oxford University Press is not responsible for the content or functionality of any supporting materials supplied by the authors. Any queries (other than missing material) should be directed to the corresponding author for the article.

This paper has been typeset from a TEX/LATEX file prepared by the author.